Archive of SID

Iranian Journal of Science & Technology, Transaction B, Engineering, Vol. 33, No. B5, pp 397-413
Printed in The Islamic Republic of Iran, 2009
© Shiraz University

# EXPERIMENTAL EVALUATION OF THE EFFECT OF EXTERNAL RESTRAINT ON BUCKLING BEHAVIOR OF THIN WELDED SHELLS*

S. ZIAEE,** M.H. KADIVAR AND K. JAFARPUR

Dept. of Mechanical Engineering, Shiraz University, Shiraz, I. R. of Iran
Email: sima_ziaee@yahoo.com

**Abstract**– Welding induces residual stresses in structures which may cause buckling distortion, if they exceed the critical buckling stress of the structure. This paper presents a predictive distortion analysis approach for a welded structure. In addition, the effect of external constraint on buckling behavior is studied, as well. A 3-D thermo-mechanical welding process simulation is performed to determine the residual stresses and deformation. Moreover, the critical buckling stress along with the buckling mode is computed through 3-D eigenvalue analysis. Also, the model is validated against the experimental work. The present results clearly demostrate that the proposed 3D welding analysis can predict not only the time, but also the shape of buckling during welding. Finally, this study also reveals that external restraint effect on buckling mode as well as a suitable combination of thickness and external restraint can eliminate buckling.

**Keywords**– Anand's model, buckling behavior, external restraint, thin shell, welding distortion

## 1. INTRODUCTION

Welding, among all mechanical joining processes, has been employed at an increasing rate for its advantage in design flexibility, cost savings, reduced overall weight and enhanced structural performance. However, welding induces various types of distortion as discussed in detail by Masubuchi [1]. To study the effect of welding on structure efficiency, and in turn to implement various distortion mitigation techniques, a valid method for predicting welding induced distortion is necessary.

Thinner section components are commonly utilized in fabricating large structures to achieve reduction in overall weight and more controllable manufacturing. However, for structures made of relatively thin components, welding can introduce significant buckling distortion, causing loss of dimensional control, structural integrity and increased fabrication costs due to poor fit-up between panels. A predictive analysis technique can determine the susceptibility of a particular design to buckling distortion.

Welding-induced buckling of thin walled structures has been investigated in great detail in [2-4]. Ueda et al. [2] presented a methodology to determine the buckling behavior of plates by large deformation elastic finite element method (FEM) and employing inherent strain distributions. Mickaleris et al. [3, 5, 6] developed a predictive buckling analysis technique for thin section panels, combining decoupled 2-D weld process simulations and 3-D eigenvalue buckling analysis. Phase transformation and transformation plasticity have also been incorporated in the analysis as shown by recent developments [7, 8].

In this work, 3-D thermo elastic-viscoplastic finite element analysis technique is applied to evaluate welding induced buckling of the welded shells. The results are checked by 3-D eigenvalue simulations and experimental data. Moreover, the effects of the shell thickness and mechanical constraints are also investigated.

*Received by the editors July 1, 2007; Accepted June 18, 2009.
**Corresponding author

www.SID.ir

Archive of SID


## 2. WELDING ANALYSIS

Welding is a coupled thermo-mechanical process and its mathematical modeling consists of two principles expressing thermal and mechanical equilibrium, i.e. the balance of internal energy and balance of momentum as well as satisfying initial and boundary conditions. To simplify the welding simulation, it is computationally efficient to perform the thermal and mechanical analysis separately [9]. Physically, it is assumed that changes in the mechanical state do not cause a change in the thermal state [9]. Computation of the temperature history during welding and subsequent cooling is completed first, and then this temperature field is applied to the mechanical model to perform residual stress analysis.

### *a) Mechanical model*

A simple set of constitutive equations for large, isotropic, visco-plastic deformations is the single-scalar internal variable model proposed by Anand [10]. Two basic features exist in the Anand model. First, this model needs no explicit yield condition and no loading/unloading criterion. Second, this model employs a single scalar as an internal variable to represent the averaged isotropic resistance to plastic flow. The inelastic strain rate $\dot{E}^P$ for the Anand model is defined by [11]:

$$\dot{\mathbf{E}}^P \equiv \widetilde{\mathbf{E}}^P(\mathbf{S}, z_1) = \dot{\varepsilon}^P \frac{\mathbf{S}}{\|\mathbf{S}\|} \quad , \qquad \dot{\varepsilon}^P = \widetilde{\varepsilon}^P(\mathbf{S}, z_1) = A \exp\left(-\frac{Q}{R\theta}\right)\left[\sinh\left(\xi \frac{\|\mathbf{S}\|}{z_1}\right)\right]^{\frac{1}{m}} \tag{1}$$

where the constitutive function $\widetilde{\varepsilon}^P$ was proposed by Anand [10]. The equations of the internal variable $z_1$ are given by [11]:

$$\begin{aligned} \dot{z}_1 &= h_0\left[1 - \frac{z_1}{z^*}\right]^a \dot{\varepsilon}^P && for \quad z_1 \le z^* \\ \dot{z}_1 &= -h_0\left[\frac{z_1}{z^*} - 1\right]^a \dot{\varepsilon}^P && for \quad z_1 \succ z^* \end{aligned} \tag{2}$$

with the criterion number

$$z^* = \bar{z}\left[\frac{\dot{\varepsilon}^P}{A}\exp\left(-\frac{Q}{R\theta}\right)\right]^{\eta} \tag{3}$$

where $A, Q, \xi, m, z, h_0, a, \bar{z}$, and $\eta$ are constants of the Anand model and $R$ is the Boltzman's constant. The material constants for the Anand model, which are used in the present work, are listed in Table 1.

Table 1. Constants of Anand's viscoplastic model for the selected material [10]

| Parameter | Value | Unit | Meaning |
|---|---|---|---|
| Z | 36.5 | Mpa | Initial value of deformation resistance |
| Q/R | $\frac{175.3}{8.314}$ | $\frac{kJ/mole}{kJ/mole \circ K}$ | $\frac{Activation\ energy}{Universal\ gas\ content}$ |
| A | 1.91e7 | $Sec^{-1}$ | Pre-exponential factor |
| $\varsigma$ | 7 | Dimension less | Multiplier of stress |
| M | 0.23348 | Dimension less | Strain rate sensitivity of stress |
| $h_0$ | 1115.6 | MPa | Hardening/softening constant |
| $\bar{z}$ | 18.9 | MPa | Coefficient for deformation resistance saturation value |
| N | .07049 | Dimension less | Strain rate sensitivity of saturation value |
| A | 1.3 | Dimension less | Strain rate sensitivity of hardening/softening |


www.SID.ir

Archive of SID



### *b) Thermal model*

Because of the small size of the melted region (weld pool) the heat source model developed by "moving isotherm pool" is used in this research.

The applied heat is transferred to the other regions by conducting through the solid materials and convection to the surroundings. During a short time in welding, the welded region remains red-colored and a portion of heat is also dissipated by radiation.

Welding time in this work is calculated by dividing the welder speed that is obtained from the practical welding characteristic data by the length of the welded region. The temperature dependent thermal properties of the material were also incorporated into the model (Table 2).

Table 2. Variation of material thermal and mechanical properties with temperature

| T($^0$C) | Thermal conductivity k(W/m.K) | Specific heat $C_p$(J/kg.K) | Coeff. of thermal expansion ($10^{-6}$) | Youngs modulus E(GPa) |
|---|---|---|---|---|
| 20 | 222 | 904 | 23.3 | 72 |
| 50 | 230 | 930 | 23.6 | 72 |
| 100 | 230 | 930 | 24 | 70 |
| 150 | 250 | 965 | 25 | 67 |
| 200 | 260 | 965 | 25 | 67 |
| 250 | 272 | 985 | 25 | 61.5 |
| 300 | 272 | 980 | 26 | 61.5 |
| 350 | 278 | 1040 | 26 | 53 |
| 400 | 278 | 1100 | 26 | 45 |
| 450 | 283 | 1100 | 26 | 45 |
| 500 | 285 | 1100 | 26 | 35 |
| 550 | 285 | 1100 | 26 | 35 |
| 600 | 320 | 1100 | 26 | 17 |
| 650 | 400 | 1100 | 26 | 10 |
| 700 | 400 | 1100 | 26 | 10 |

### *c) Finite element approximation*

The finite element method for uncoupled thermo-mechanical problem is based on the Ritz's approximation of variational equation, i.e. the principle of virtual work and the balance of internal energy.

The combined global finite element equation for the uncoupled thermo-mechanical problem is expressed by

$$\begin{bmatrix} \mathbf{K}_u^n & \mathbf{K}_{u\theta}^n \\ \mathbf{0} & \frac{1}{\Delta t}\mathbf{C}^n + \mathbf{K}_\theta^n \end{bmatrix} \begin{bmatrix} \Delta \mathbf{u} \\ \Delta \theta \end{bmatrix}^i = \begin{bmatrix} \mathbf{R}_u^{n+1} \\ \mathbf{R}_\theta^{n+1} \end{bmatrix} - \begin{bmatrix} \mathbf{F}_u^{n+1} \\ \mathbf{F}_\theta^{n+1} \end{bmatrix}^{(i-1)} \tag{4}$$

where $\mathbf{K}_u^n$ is the stiffness matrix corresponding to mechanical effects, $\mathbf{K}_{u\theta}^n$ is the matrix which transforms thermal energy into a mechanical one. The thermal stiffness $\mathbf{K}_\theta^n$ is the sum of stiffness matrix corresponding to conduction, the stiffness related to convection phenomena, and the stiffness associated with radiation effects. $\Delta \mathbf{u}|_{(i)}$ and $\Delta\theta\big|_i$ are the vector of displacement and temperature increments, respectively; $\mathbf{R}_u^{n+1}$ is the vector of externally applied nodal point loads, $\mathbf{F}_u{}^{n+1}|_{i-1}$ is the vector of nodal point forces equivalent to the internal stresses. $\mathbf{R}_\theta^{n+1}$ is the summation of vectors of nodal thermal loads corresponding to the thermal boundary condition. $\mathbf{F}_\theta^{n+1}\big|_{i-1}$ is the vector of nodal thermal loads corresponding to the internal heat flux through the body surface $\partial V$.



www.SID.ir

Archive of SID


The matrixes in equation (4) are taken at the current, n+1, and previous, n, time steps and current, (i), and previous, (i-1) iterations at the current time step.

The nonlinear finite element system of equations is solved iteratively by Newton-Raphson scheme.

***d) Element rebirth technique***

If material is added to (or removed from) a system, certain elements in the model may become "existent" (or "nonexistent"). The element birth and death options can be used to deactivate or reactivate selected elements in such cases. To achieve the "element death" effect, the program does not actually remove "killed" elements. Instead, it deactivates them by multiplying their stiffness (or conductivity, or other analogous quality) by a severe reduction factor. This factor is usually set to a small value (order of 10e-6). Element loads associated with deactivated elements are zeroed out of the load vector. Similarly, mass, damping, specific heat and other such effects are set zero for deactivated elements. The mass and energy of deactivated elements are not included in summations over the model. An element's strain is also set to zero as soon as that element is killed.

In a like manner, when elements are "born", they are not actually added to the model; they are simply reactivated. When an element is reactivated, its stiffness, mass, element loads, etc, return to their full original values.

## 3. THREE-DIMENSIONAL EIGENVALUE ANALYSIS

The buckling distortion and critical buckling stresses are consequently determined by an eigenvalue analysis applying the mostly uniform and compressive longitudinal plastic strain field of the 3-D weld model on the 3-D structural model as equivalent load.

Michaleris et al. [3,6] applied a constant, negative thermal load at the weld region to introduce the effect of welding into 3-D structures. Thermal loading is used rather than mapping the plastic strain field, which would require a complex analysis procedure; after that, an eigenvalue analysis is performed to determine the critical residual stresses and buckling distortion. This value is then compared with the longitudinal residual stress that is obtained by 2D finite element analysis of welding. Finally, the ability of this method to estimate the critical stresses and buckling mode is evaluated by experimental data [3, 6]. The proposed method by Michaleris only predicts if the plate buckles or not and is silent about the time of buckling and the behavior of the plate after buckling.

In the present work, the actual stress pattern of the shell in each time step is used in 3D eigenvalue analysis to determine the critical residual stresses and to estimate the time of buckling (during and/ or after opening the fixtures). Then, the outcome is used to find a simple way to estimate buckling with 3D welded analysis. To validate the results, an experimental method is designed and used.

## 4. VALIDITY OF MODEL

To check the accuracy of the proposed method, a specimen was constructed with a length, width and thickness of L=1800, W= 300, t= 1.5 mm, respectively. Figure 1 shows the variation of longitudinal residual stress of a middle point of the shell with respect to time for the present model and Pattee's experimental work [12]. As Fig. 1 illustrates, the variation of computed stress has a pattern similar to the pattern of experimental data and shows a good compatibility between the results. Therefore, the procedure presented here is suitable for analysis of transient and residual stresses due to welds.


www.SID.ir

Archive of SID



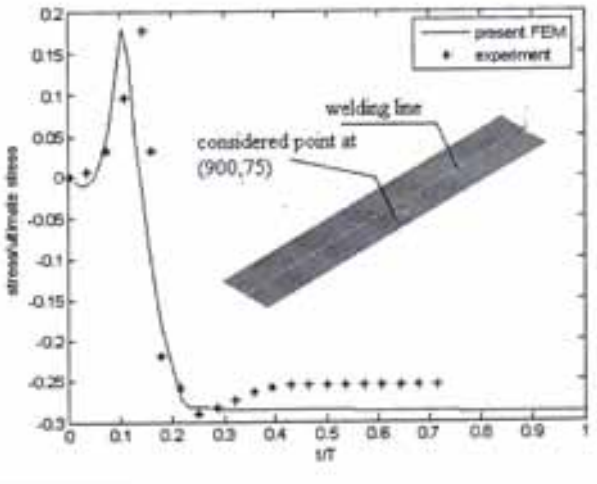


Fig. 1. Comparison between the present method and the experimental data of [12]

## 5. MODEL ANALYSIS

In this work, two thin wall shell sections are jointed by a single pass butt welded. The length, width, thickness, and radius of the shell are assumed to be 500, 250, 1.5 and 1000 mm, respectively. Seven thousand 3D elements are used to construct the model. Fine meshes are used near the weld line and with increasing distance from the weld line the mesh density is decreased. In order to obtain a highly precise prediction of welding distortion, material nonlinearity (thermo-viscoplastic), geometrical nonlinearity (large deformation), and contact nonlinearity are taken into account. However, uncoupled thermo-mechanical analysis is used to save computational time. The mechanical properties are dependent on the temperature history as listed in Table 1.

## 6. EXPERIMENTAL MODELS

In order to validate the results of the proposed finite element method, some experiments are designed. The experimental models are constructed of Al100, and its mechanical properties listed in Table 1.The experimental models are welded using TIG method, the details of which will be given in the next section. Welding parameters are shown in Table 3. The emphasis on the experimental part was to observe the behavior of the welded shells during welding without fixtures or with fixtures at different positions.

Table 3. Welding parameters

| | |
|---|---|
| Voltage | 8-10 Volts |
| Current | 90 Amps |
| Travel speed (Average) | 254mm/minute |

## 7. RESULTS

To evaluate the response of a welded structure, elastic small deformation eigenvalue analysis is suggested. Small deformation analysis requires limited computational resources, and for this reason, it cannot predict buckling behavior. However, here it is only used to estimate the stress pattern that causes buckling in each time-step of welding. For this purpose, the actual stress pattern of the shell is used in 3D-eigenvalue analysis in each time-step of welding and the time of buckling is the time step in which the smallest produced eigenvalue is smaller or equal to 1. It is predicted that the shape of the buckling mode is very similar to the eigenmode corresponding to the nearest eigenvalue equal to 1.



www.SID.ir

Archive of SID


***Case 1: free-free 1.5 mm shell-*** According to 3D-eigenvalue analysis using the true stress pattern of shells produced by 3D-thermo-viscoplastic, the thin shell loses its stability two times during the welding, the first one occurs 36s after starting welding ($\lambda$=0.94), and the second is seen at time 60s ($\lambda$=1.006). The predicted shape of the buckling mode belonging to the first instability (the eigenmode of $\lambda$=0.94) is shown in Fig. 2a. Figure 2b reveals the shape of the welded shells exactly after buckling time. Comparison between Fig. 2a and Fig. 2b shows some similarities between the predicted eigenmode and the deformed shape of the welded shells at the time of buckling. Angular deformation and a bight near the weld line are seen in both of the deformed shapes. Reviewing the history of deformation would reveal that most of the shell points have a sudden variation in the radial direction at buckling time (comparison between Fig. 2b and Fig. 2c) as Masubuchi has pointed out [1]. This behavior is repeated at the second buckling of the welded shells.

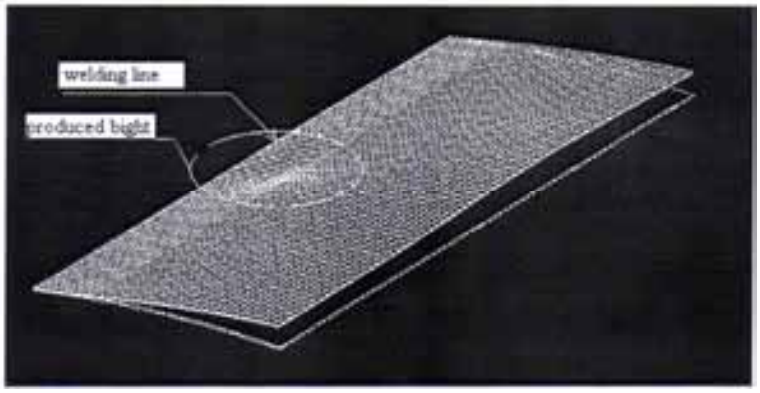


a) Eigenmode belong to the first instability of welded shells which is predicted by 3D-eigenvalue analysis


b) Deformed shape of welded shells exactly after the first buckling(scale 1)

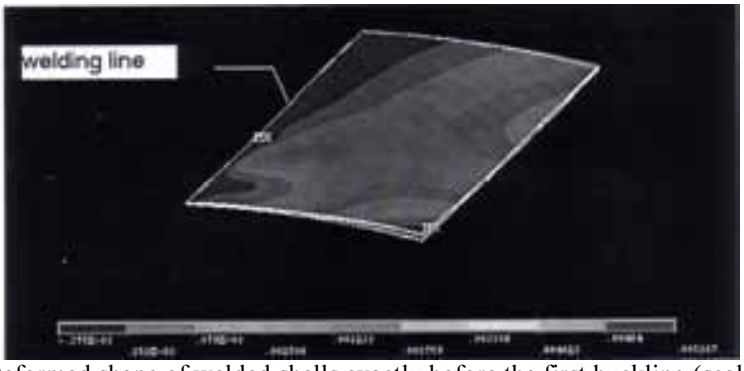


c) Deformed shape of welded shells exactly before the first buckling (scale 1)

Fig. 2. Comparison between the deformed shape of welded shells at time of buckling produced by 3D-thermo-vicoplastic analysis and predicted eigenmode produced by 3D-eigenvalue analysis


www.SID.ir

Archive of SID



Both buckling modes are very similar, a sudden jump at the edge of shell and appearance of a new cavity near the weld are special characteristics of buckling modes. After the welding is cooled down, two complete sine wave and one half wave are seen near the weld line (Fig. 3a and 4b2) and only a sine wave is beheld near the edge (Fig. 3a) and 4b1), moreover, angular distortion due to buckling is noticeable as well (Fig. 3a).

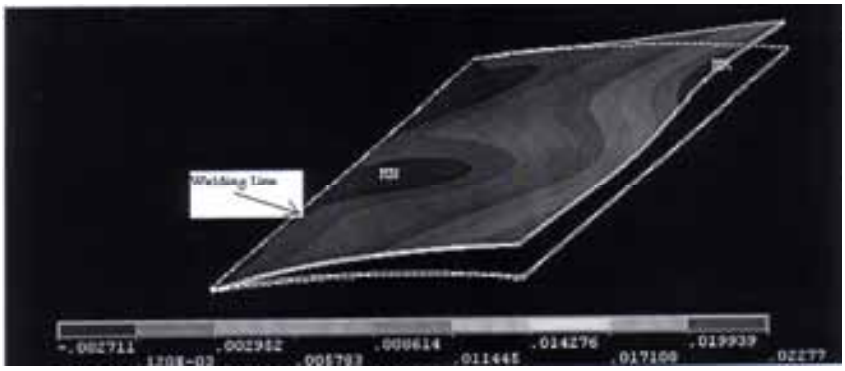


a) The final deformed shape of thin shell after buckling two times, based on the proposed 3D analysis

b) Present experimental result

c) Out of plane displacement is nearly 2cm in this present experiment

Fig. 3. The final deformed shape of thin shell. a) proposed 3D analysis. b,c) present experiment results

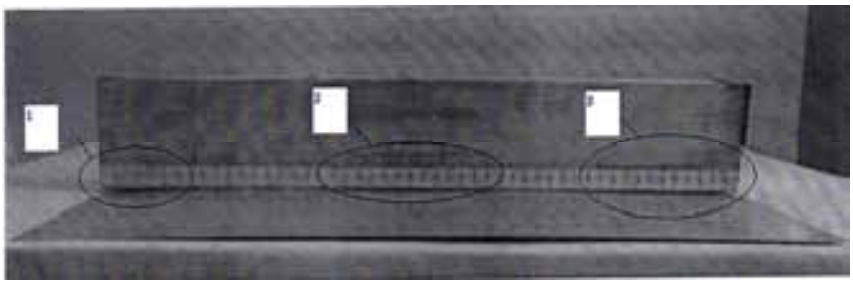

a) Present experiment

1) The first dimpling 2) The middle dimpling 3) The last dimpling

b-1. The wave shape of edge (scale 1) b-2. The wave shape of upper portion (scale 7)

Fig. 4. Comparison between the wave shape of the upper portion of the shell (near weld) and its edge. a) present experiment results (the wave of upper portion is shown with a ruler) b) proposed analysis



www.SID.ir

Archive of SID


Twenty seconds after welding has started, sudden variation in the radial direction can be observed at a small zone of shell near the weld line and a hilly shape is produced. This accident has less influence on the overall deformation of the welded shells. Figure 5 shows the difference between the deformation of this area before and after local buckling with the use of two perpendicular strips. It is easily seen that borderline nodes do not experience out of plane displacement. Then, one can isolate this area with the use of simply support boundary condition and determine if the true stress distribution belonging to this area can lead to its buckling. Eigenvalue analysis gives a positive answer to this question ($\lambda = 0.8$). Then, one can classify this phenomenon as local buckling and exactly 16s after that, the first global buckling occurs. This behavior is seen after 52s again.

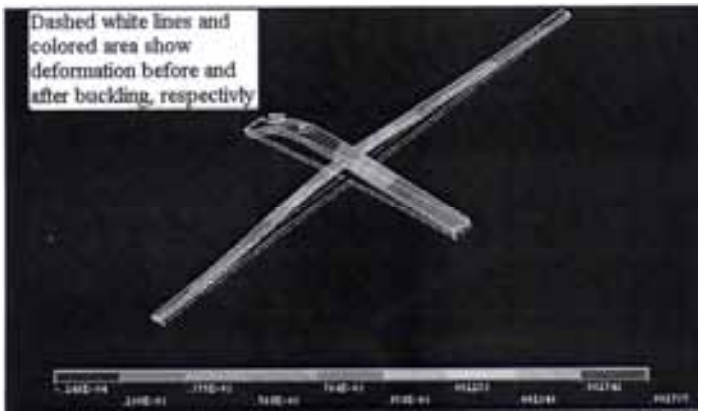


Fig. 5. Isolated local buckling area. Perpendicular strips are used for a better comparison between displacements before buckling and after buckling

Figure 6 shows the shape of the upper portion of the shell after the second local buckling occurs. Thus, the wave shape near the weld line is produced by a combination of global and local buckling of shells during welding. With the use of the present experimental data, the correctness of the result is confirmed. The final shape of the buckling mode that is obtained by the experimental method is shown in Fig. 3b. Also, the difference between the shape of the edge and the upper portion of the shell, near the weld line that are produced by the experiment and the proposed finite element method is illustrated in Fig. 4. Based on this figure, one can see some similarities between the wave shapes produced by the experiment and the proposed finite element model. According to Fig. 4a, the wave near the weld line is smaller than the wave near the edge and has a sine shape. Because of the symmetrical response, only one half of the finite element model is shown in all figures. In comparison, between the out of plane displacement of the edge that is produced by the experiment (Fig. 3c), and the proposed FEM (Fig. 3a), the amount of error may be estimated to be around 15.7%.

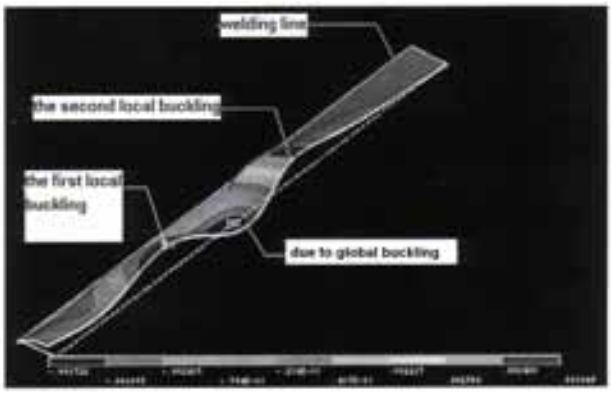


Fig. 6. Deformed shape of shell (near the weld line) after the second local buckling. (Scale 7.5)


www.SID.ir

Archive of SID



Based on the work of other researchers [1, 5, 6,12] who believe longitudinal residual stresses can lead to buckling of weldments, the approximated longitudinal transient stresses that are produced in each time step are applied to 3D-eigenvalue analysis to predict buckling time and corresponding eigenmode. Although this method repeated the same buckling times, some differences are seen in the predicted eigenmodes. Figure 7 shows the predicted eigenmode belongs to the first buckling of welded shells.

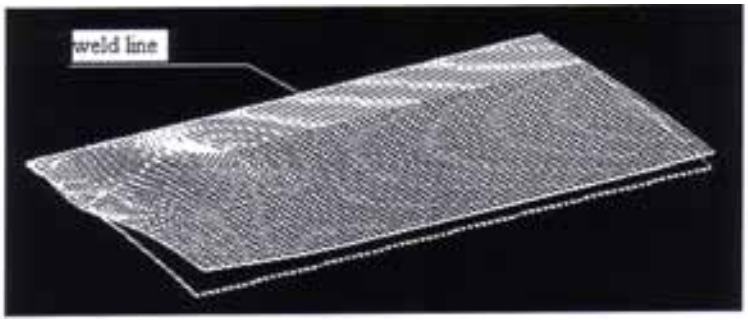


Fig. 7. Eigenmode predicted by applying approximated longitudinal transient stresses to 3D-eigenvalue analysis

Comparison between Fig. 7 and Fig. 2a clearly reveals that one can predict buckling time and approximated buckling shape using longitudinal transient stresses. This shows the importance of longitudinal stresses in buckling occurrence. Distribution of longitudinal residual stresses (due to welding and buckling) is shown in Fig. 8. Except for points near the weld line, other points experience compressive longitudinal stress, as was expected.

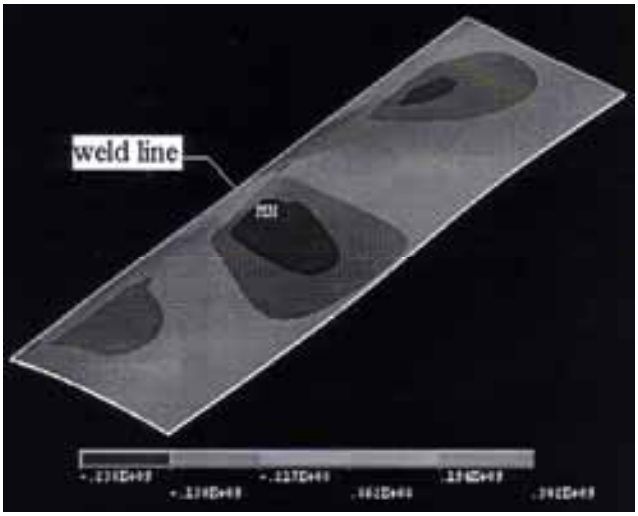


Fig. 8. Distribution of longitudinal residual stress

***Case 2 free-fixed 1.5 mm shell-*** The global buckling of free-fixed shell occurs at 24s after the welding has started. Sudden angular distortion and the tendency of the weld line to become erected from its support are the characteristics of the buckling mode. Eigenvalue analysis confirms the time of buckling. Continuing welding induces the space between the shells and inferior support to increase. This deformation is similar to the first mode of fixed-free beam under concentrated compression load. Figure 9 and 10 show the comparison between the analytical and experimental shapes of the welded shells before and after removing the torch, respectively. This mechanical constraint does not eliminate local buckling and can be seen around arc welds.



www.SID.ir

Archive of SID


a) Obtained by proposed FEM b) Experiment

Fig. 9. The front view of deformed welded shells exactly before removing torch.

a) Obtained by proposed FEM b) Experiment

Fig. 10. The lateral view of deformed welded line exactly after removing torch

Figure 11 shows the distribution of longitudinal stress mid line of the shells three times (before buckling and at the time of buckling) when the torch has not reached the mid line of the shells yet. This figure clearly reveals rapid growth of longitudinal compressive stresses near the weld line at the time of buckling. At this time, most of the area near the weld line (especially the area ahead of the torch) experiences compressive longitudinal stresses (Fig. 11) and it seems that this distribution of longitudinal stress is enough to buckle the shells (based on eigenvalue analysis).

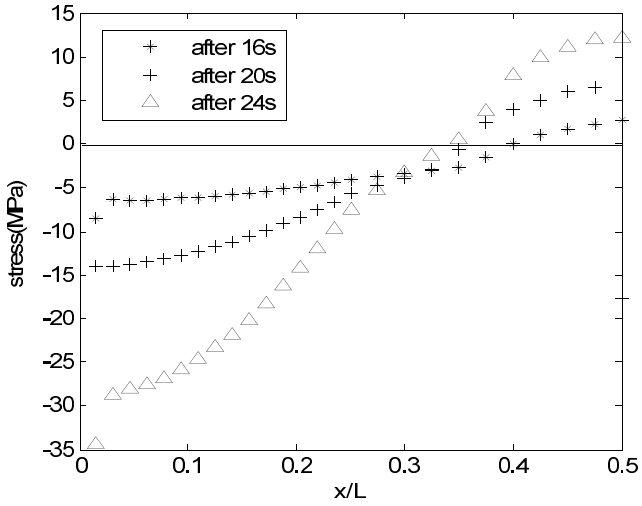


Fig. 11. Distribution of longitudinal stress along the line mid space of the shell three times after welding has started. x and L are distance from weld line and total width of shell, respectively

After completing the cooling stage, only the angular distortion due to buckling remains and the shells lie on their support. Figure 12 shows the front view of shells after completed cooling. Experiment verifies this phenomenon.

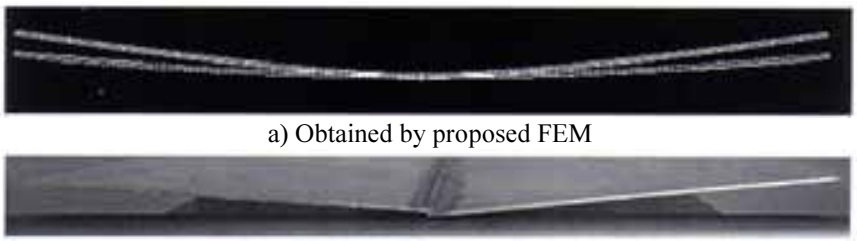

a) Obtained by proposed FEM

b) Produced by experiment

Fig. 12. Front view of final shape distortion after cooling stage


www.SID.ir

Archive of SID



Figure 13 reveals the distribution of longitudinal stress after completing the cooling stage. The comparison between Fig. 8 and 13 clearly shows that changing boundary condition influences the distribution and magnitude of stress and it can be a good explanation for the difference between the produced final buckling modes.

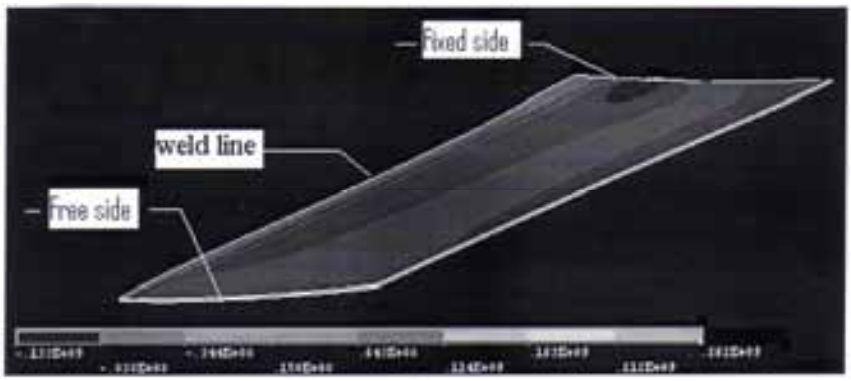


Fig. 13. Distribution of longitudinal residual stress at free-fixed welded shells

***Case 3 fixed-fixed (perpendicular to weld line) 1.5 mm shell-*** The fixed-fixed shell experiences six different local bucklings during the welding. The first one occurs 4s after starting welding and the last is at 52s, which is coincident with the time of the last buckling of the free-free shell. The first local buckling of fixed-fixed and free-free shell is similar, but the last ones are different; one of them is concave and the other is convex. Finally, two complete waves are seen on the upper portion of the shell. Figure 14 illustrates the shape of the shell after the last local buckling is being generated.

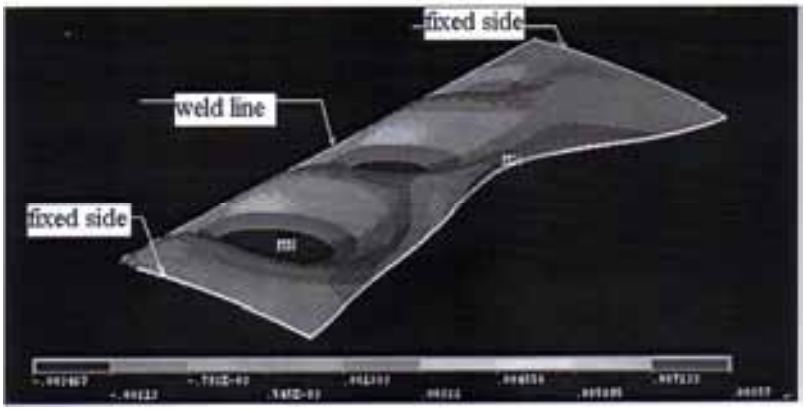


Fig. 14. Shape of shell after producing the last local buckling (scale 7.5)

At the end of welding and after the shells have been cooled down with the fixtures removed from the sides, the overall jump showing the first global buckling of the shell after cooling is seen. Figure 15 and 16 show the distribution of longitudinal stress before the fixtures are removed and the buckling mode of the shells after that, respectively. Eigenvalue analysis and experiment confirm the buckling time. Of course, buckling mode is verified by experiment (Fig. 17 and Fig. 16 show similar deformation especially at the marked zones).

***Case 4 fixed-fixed (parallel to weld line) 1.5mm shell -*** In this case, instead of sides that are perpendicular to the weld line (case 3), parallel sides with the weld line are fixed. Although this case does not experience global buckling until before removing fixtures (like case 3), the mode shape is completely different. The comparison between the longitudinal compression stresses shows the position of the external constraint influences on the distribution and value of longitudinal stresses. This fact can explain the difference



www.SID.ir

Archive of SID


between the resultant mode shapes. Figure 18 shows the analytical and experimental mode shape of the shells after removing the fixtures. Eigenvalue analyses also ratify the time and the mode of buckling.

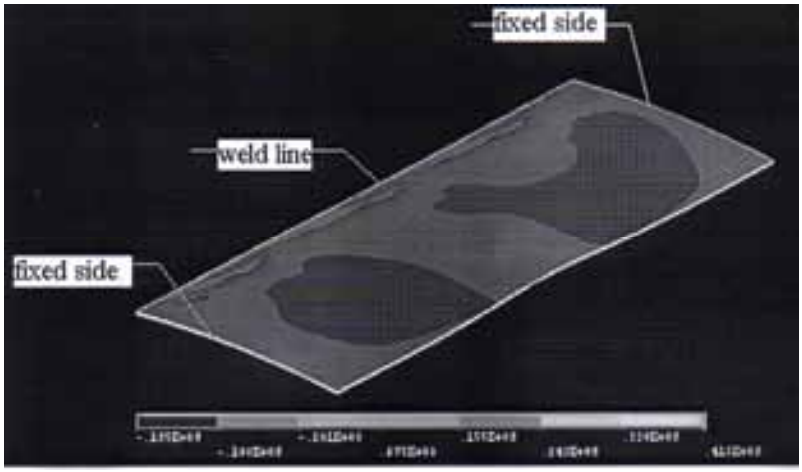


Fig. 15. Distribution of longitudinal stress before fixture removal

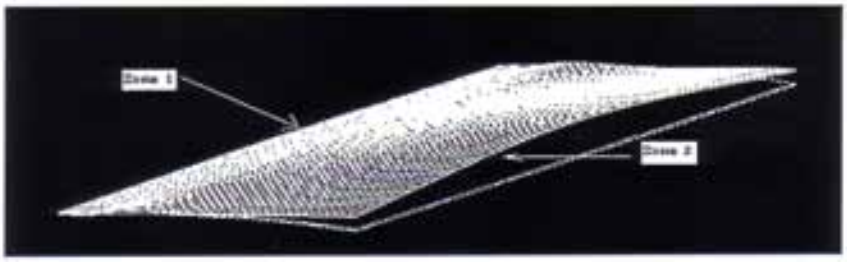

a)Overall shape of buckling mode

b) Deformed shape near weld line

Fig. 16. Mode shape of shells after fixture removal

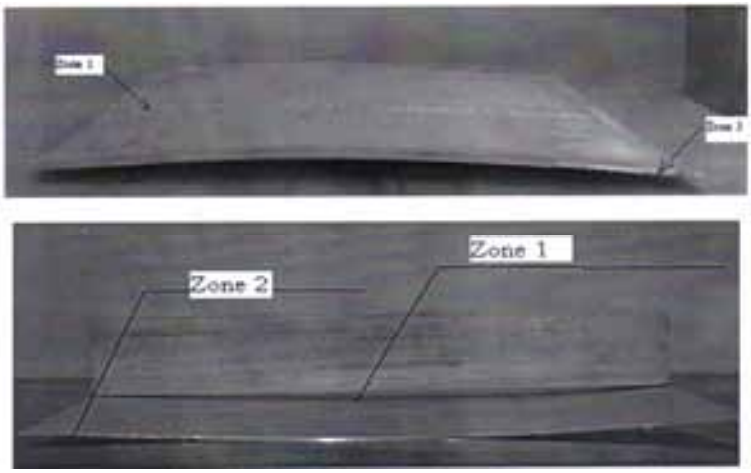


Fig. 17. Experimental deformed shape of shells after fixture removal


www.SID.ir

Archive of SID




a) Mode shape of shells after fixtures removal

b) Experimental deformed shape of shells after fixture removal

Fig. 18. Comparison between mode shape of welded shells produced by FEM and experiment

In this case local buckling can be seen during the welding and their location is around the weld torch.

This case and case number 3 both only experience local buckling during welding, and after removing fixtures their equilibrium shapes change and they buckle. Although magnitude and distribution of compressive residual stress belonging to these cases are different (Fig.19 and Fig.15), both of them are more than the critical compressive residual longitudinal stresses of free-free welded shells and less than the critical values that belong to the restrained shells. So these welded shells do not experience buckling until removing the fixtures, but exactly with opening fixtures, buckling occurs. This means that the pattern of stress at the moment of opening fixtures is enough for buckling and the difference between the pattern and magnitude of residual stress leads to the difference between the produced mode shapes. The magnitude of residual longitudinal stresses changes after establishing the new shape of welded shells. Figure 20 shows the time history of the longitudinal stress of different nodes along the mid line of the shell in case 4. This figure clearly reveals that after removing the fixtures and in the new equilibrium path of welded shells, the magnitude of compressive residual longitudinal stress is reduced.

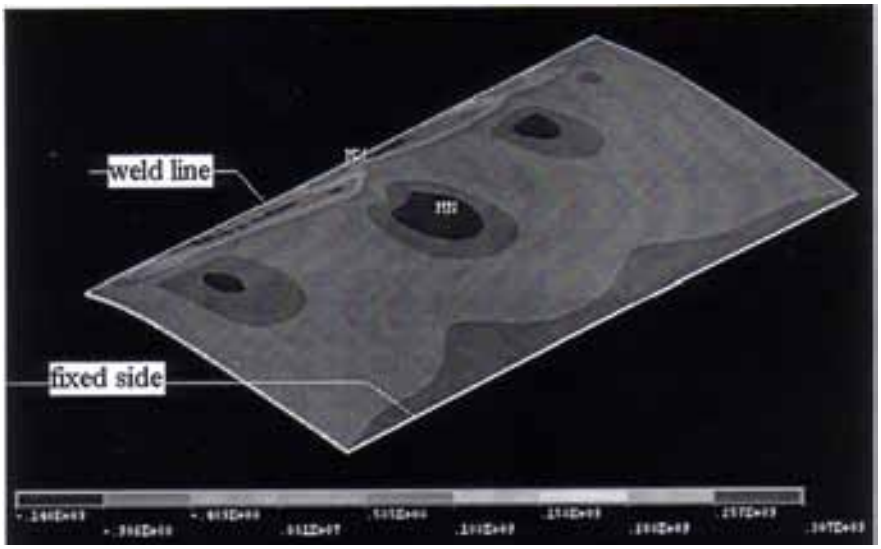


Fig. 19. Distribution of longitudinal stress before fixture removal



www.SID.ir

Archive of SID


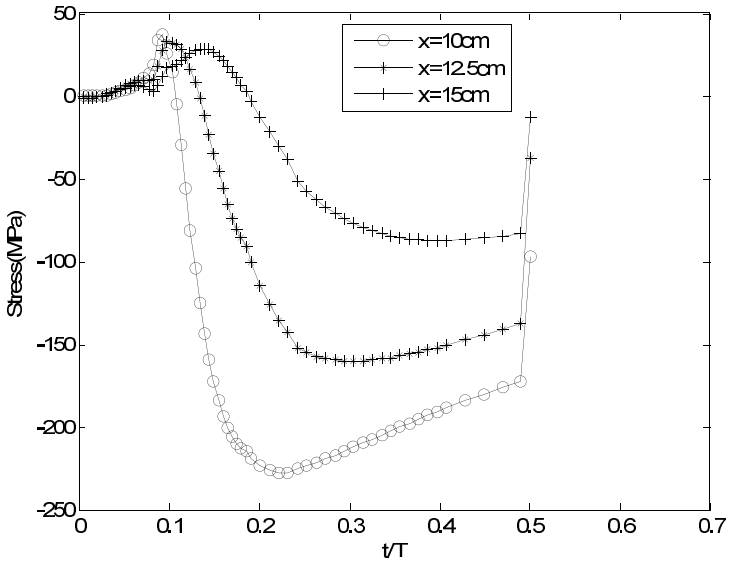


Fig. 20. Time history of some nodes along the mid line of shell. Parameter x represents the distance from weld line

***Case 5 fully restrained 1.5mm shell-*** In this case four sides of shells were restrained only in the radial direction (zero out of plane displacements at these places). Figure 21 shows the distribution of longitudinal residual stress after completing the cooling stage. Comparison of this figure with Fig. 15 clearly displays many similarities in distribution and magnitude of stress. This case experiences buckling after removing fixtures too, and its final shape mode is very similar to case 3. Figure 22(a) shows this mode shape. The experiment verifies this prediction (Fig. 22b).

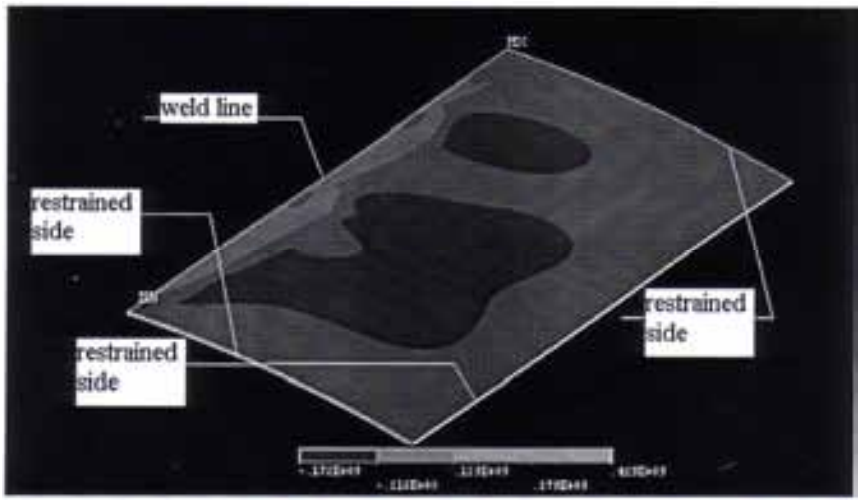


Fig. 21. Distribution of residual longitudinal stress after completing cooling and before removing fixtures

***Case 6 free-free 3mm shell-*** By increasing the thickness of the shell local buckling is eliminated, but 76 seconds after starting welding, overall jumping can be seen and the shell loses its stability (Fig. 23). The correctness of this prediction can be seen by comparison between this method and the Michaleris method [3, 6]. The average stress at the middle of the shell, exactly before buckling, is 45MPa and the Michaleris' method [3, 6] predicts the critical stress near 39 MPa for this case.


www.SID.ir

Archive of SID



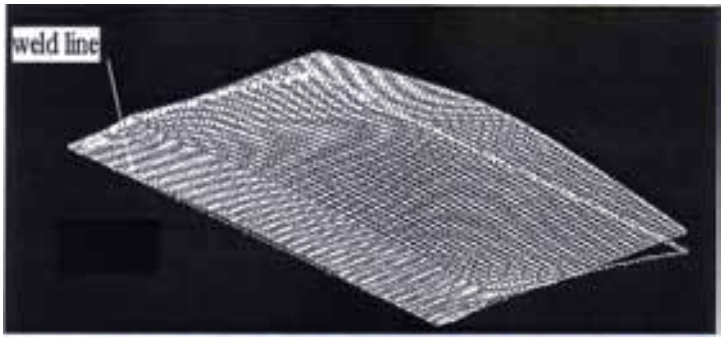


a) Produced by FEM

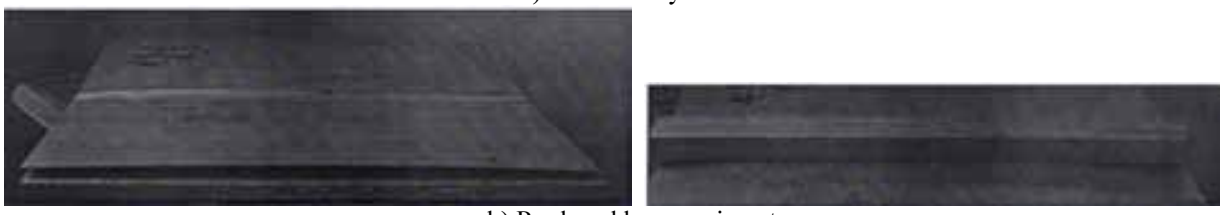

b) Produced by experiment

Fig. 22. Mode shape of welded shells after opening fixtures

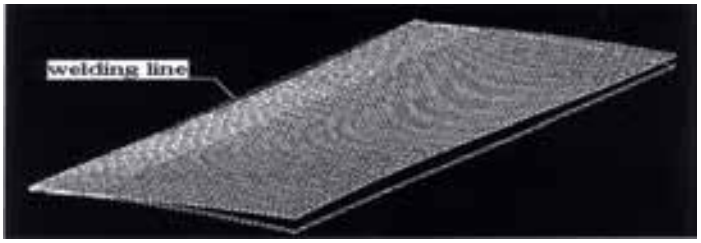


Fig. 23. buckling shape of 3mm shell

***Case 7 fully fixed 3mm shell-*** In the last example, the buckling behavior of the 3mm shell with fully fixed boundary conditions is analyzed. By increasing the thickness of the shell not only global buckling, but also local buckling are eliminated and no jump (overall or local) can be seen during welding and after opening the fixtures (Fig. 24). The average stress at the middle of the shell, after cooling and opening three sides, is 32.8 MPa and it is smaller than the smallest critical stresses that are predicted by the Michaleris method [3, 6] for different boundary conditions of shell (76 MPa for free-fixed and 39MPa for free-free conditions). On the basis of this comparison, the correctness of the prediction is confirmed.

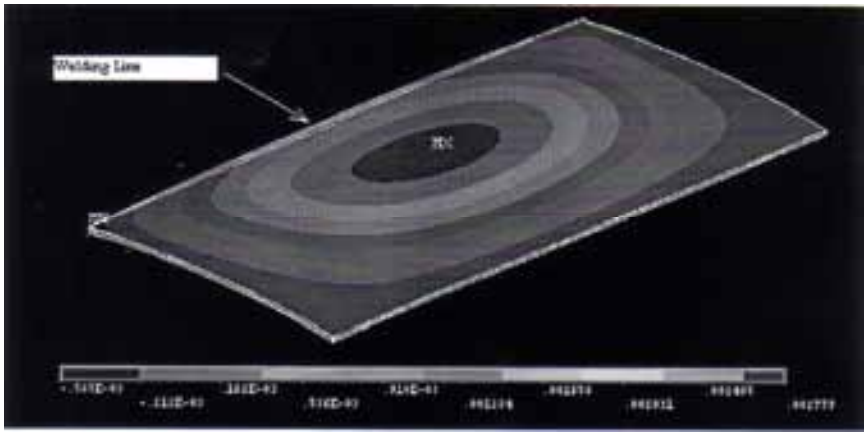

Fig. 24. The final deformed shape of thin shell



www.SID.ir

Archive of SID


## 8. CONCLUSION

In this work, welding distortions, especially buckling behavior, is studied with the use of 3D thermo-elastic visco-plastic finite element analysis. Also, the effects of external constraint and thickness on buckling behavior are evaluated. On the basis of the proposed model, one can clearly evaluate not only the buckling shape, but also the time of buckling. It is seen that the sudden variation of out of plane displacement almost always occurs during buckling. If buckling occurs during welding, the proposed model allows behavior evaluation of weldments after buckling. In addition, the results clearly show that thickness and external constraints are effective on the buckling resistance of shells. Although both parameters increase buckling resistance they can not eliminate buckling alone. In the case of the shells 1.5mm thick, with changing boundary conditions, global buckling can be eliminated during the welding but it is seen after opening the fixtures. Also, boundary conditions are ineffective on local buckling. It is seen that the buckling is more localized in the welded shells 1.5mm thick. Each zone of shell that experiences compressive longitudinal stresses greater than the critical ones and having a size around half of the wave length loses its stability. These zones can be found near the weld line and approximately around the weld torch because of the created transient compressive longitudinal stresses in this area during the welding. It is seen that changing boundary conditions in the case of shells 1.5 mm thick changes the mode shape of buckling because of varying the value and distribution of longitudinal compressive stress. An increase in the thickness (from 1.5mm to 3mm) only omits the local buckling, but if it is combined with suitable boundary conditions, the global buckling can be eliminated, too. Proper restraints can increase buckling strength and prevent it during welding, and if the produced residual stresses after cooling the weldments are smaller than the critical stresses, buckling will not be seen after the fixtures are removed. Thus, buckling of shell due to welds can be omitted by using a suitable combination of thickness and external constraint.

## REFERENCES


1. Masubuchi, K. (1980). *Analysis of welded structures*. Pergamon Press, Oxford.
2. Murakawa, H., Ueda, Y. & Zhong, X. M. (1995). Buckling behavior of plates under idealized inherent strain. *Transactions of JWRI*, Vol. 24, No. 2, pp. 87-91.
3. Michaleris, P. & Debiccari, A. (1997). Prediction of welding distortion. *Welding Journal*, Vol. 76, No. 4, pp. 172-180.
4. Tsai, C. L., Park, S. C. & Cheng, W. T. (1999). Welding distortion of a thin-plate panel structure. A.W.S., *Welding Journal*, Research Supplement, Vol. 78, pp. 156s-165s.
5. Michaleris, P. & Debiccari, A. (1996). A predictive technique for buckling analysis of thin section panels due to welding. *Journal of Ship Production*, Vol. 12, No. 4, pp. 269-275.
6. Michaleris, P., Deo, M. V. & Sun, J. (2003). Prediction of buckling distortion of welded structures. *Science and Technology of Welding & Joining*, Vol. 8, No. 1, pp. 55-61.
7. Oddy, A. S., Goldak, J. A. & McDill, J. M. J. (1990). Numerical analysis of transformation plasticity in 3D finite element analysis of welds. *European Journal of Mechanics,A/Solids*, Vol. 9, No. 3, pp. 253-263.
8. Watt, D. F., Coon, L., Bibby, M. & Henwood, C. (1988). An algorithm for modeling microstructural development in weld heat affected zones (part a) reaction kinetics. *Acta Metal*., Vol. 36, No. 11, pp. 3029-3035.
9. Ziaee, S., Kadivar, M. H. & Jafarpur, K. (2008). A sequence scheme to reduce the residual stresses in welding of circular elements. *Iranian Journal of Science & Technology, Transaction B, Engineering*, Vol. 32, No. B4, pp. 367-383



www.SID.ir

Archive of SID



10. Brown, S. B., Kim, K. H. & Anand, L. (1989). An internal variable constitutive model for hot working of metals. *International Journal of Plasticity*, Vol. 5, pp. 95-130
11. Ronda, J. & Oliver, G. J. (1998). Comparison of applicability of various thermo-viscoplastic constitutive models in modeling of welding. *Comput. Methods Appl. Mech. Engrg*., Vol. 153, pp. 195-221.
12. Pattee, F. M. (1975). Buckling distortion of thin aluminium plates during welding. Thesis, Master of Science, Massachusetts Institute of Technology.



www.SID.ir